RMCProfile: reverse Monte Carlo for polycrystalline materials

2007 J. Phys.: Condens. Matter 19 335218

(http://iopscience.iop.org/0953-8984/19/33/335218)

IOP PUBLISHING JOURNAL OF PHYSICS: CONDENSED MATTER

J. Phys.: Condens. Matter **19** (2007) 335218 (16pp) doi:10.1088/0953-8984/19/33/335218

RMCProfile: reverse Monte Carlo for polycrystalline materials

Matthew G Tucker[1], David A Keen[1], Martin T Dove[2], Andrew L Goodwin[2] and Qun Hui[2,3]

[1] ISIS Facility, Rutherford Appleton Laboratory, Chilton, Didcot, Oxfordshire OX11 0QX, UK
[2] Mineral Physics Group, Department of Earth Sciences, University of Cambridge, Downing Street, Cambridge CB2 3EQ, UK

E-mail: m.g.tucker@rl.ac.uk

Received 22 March 2007
Published 4 July 2007
Online at stacks.iop.org/JPhysCM/19/335218

Abstract

A new approach to the reverse Monte Carlo analysis of total scattering data from polycrystalline materials is presented. The essential new feature is the incorporation of an explicit analysis of the Bragg peaks using a profile refinement, taking account of the instrument resolution function. Other new features including fitting data from magnetic materials, modelling lattice site disorder and new restraint and constraint options. The new method is demonstrated by a brief review of studies carried out during its development. The new program `RMCProfile` represents a significant advance in the analysis of polycrystalline total scattering data, especially where the local structure is to be explored within the true constraints of the long-range average structure.

(Some figures in this article are in colour only in the electronic version)

1. Introduction

The development of the reverse Monte Carlo (RMC) method [1, 2] was strongly motivated by the need for a tool to develop models of the structures of liquid and amorphous phases from neutron and x-ray total scattering data. These states of matter are unlike crystalline materials, for which Bragg peak positions and intensities can provide information about the crystal lattice and the average positions of atoms within the crystal unit cell. The RMC method involves adjusting the positions of a large number of atoms in an ensemble guided by the comparison of the calculated total scattering pattern and/or the pair distribution function with the experimental data, using a Monte Carlo algorithm.

Although the RMC method was envisaged as a tool for the study of liquid and amorphous materials, it has been applied to the study of crystalline materials and in particular to the study of disordered crystals, where there is often a significant difference between the

[3] Present address: Southwest University, Mianyang, Sichuan, People's Republic of China.

long-range average structure and the short-range structure [3–6]. Examples include fast-ion conductors, orientationally disordered molecular crystals and framework structures with orientational disorder of the linked atomic polyhedra. The RMC approach can be used in its standard mode [1], but this both minimizes and degrades the value of the specific information contained within the Bragg peaks. The explicit use of the Bragg peaks is important because they contain direct information about the mean distribution of atom positions in the unit cell, which in crystallographic terms is represented by mean positions and displacement distribution functions, the latter of which are often represented by Gaussian functions. This is in contrast to the total scattering data, which contain information about the pair distribution functions. By combining the two types of data it is possible to obtain information about both the long-range and short-range order of a structure. In disordered crystalline materials, the short-range order will represent large-amplitude local fluctuations of the atoms away from their mean positions. The use of Bragg scattering intensities also allows the RMC method to make use of the three-dimensional nature of Bragg diffraction. Although with polycrystalline samples the three-dimensional Bragg scattering is projected onto a one-dimensional measurement, it is possible to identify a three-dimensional scattering vector $\mathbf{Q}_{hkl}$ with each reflection, just as Rietveld refinement [7] of powder diffraction data gives three-dimensional structural information.

New instruments at neutron spallation sources and x-ray synchrotron sources are now providing total scattering data of very high quality to large values of the scattering vector $\mathbf{Q}$. One such instrument is the general materials diffractometer (GEM) at ISIS [8]. This instrument has been optimized to study both crystalline and amorphous materials and can provide very high-quality powder diffraction data to a $Q_{\max}$ of 50 Å^{-1}. Clearly any new RMC method needs to be able to fully exploit these data to provide the most accurate information about the polycrystalline materials being studied.

There have been two adaptations of the RMC method for the study of polycrystalline materials [3, 5] and these will be discussed below. In this article a third adaptation is presented, which is based on profile fitting of the Bragg diffraction data [4]. This new method encompasses the key capabilities of the previous versions and for high-Q data from neutron spallation and x-ray synchrotron sources will supersede them in most applications. For completeness, we note that the `PDFfit` method [9] has also been used to study local disorder within crystalline materials. `PDFfit` is a 'real-space Rietveld' method with particular applicability to areas such as Jann–Teller distortions in perovskites and nanocrystalline materials (see Egami and Billinge [10] for further details).

The remainder of the paper is organized as follows. First the basic formalism underpinning the RMC methods is set out and previous RMC methods specifically designed for crystalline materials are described. This is followed by a detailed description of the new RMC method (which is incorporated into the program `RMCProfile`) and its capabilities. Finally a set of example studies using this new method is presented.

2. Formalism

2.1. Neutron total scattering

It is useful at the outset to outline the formalism of total scattering; here we follow the formalism reviewed by Keen [11]. The total scattering intensity is given by

$$\frac{1}{N}\frac{\mathrm{d}\sigma}{\mathrm{d}\Omega} = F(Q) + \sum_{j=1}^{n} c_j \overline{b^2}_j \tag{1}$$

where $4\pi \sum_j c_j \overline{b^2}_j$ is the total scattering cross-section of the material and the summation is over the n atom types. There are N atoms in the material and c_j is the proportion of atom type j. $F(Q)$, the total scattering structure factor, is related to the total radial distribution function, $G(r)$, by the Fourier transforms

$$F(Q) = \rho_0 \int_0^\infty 4\pi r^2 G(r) \frac{\sin Qr}{Qr} \, \mathrm{d}r \tag{2}$$

$$G(r) = \frac{1}{(2\pi)^3 \rho_0} \int_0^\infty 4\pi Q^2 F(Q) \frac{\sin Qr}{Qr} \, \mathrm{d}Q \tag{3}$$

with average atom number density $\rho_0 = N/V$ (in atoms Å^{-3}). $G(r)$ is defined by the partial radial distribution functions $g_{ij}(r)$:

$$G(r) = \sum_{i,j=1}^{n} c_i c_j \overline{b}_i \overline{b}_j \left(g_{ij}(r) - 1 \right) \tag{4}$$

where

$$g_{ij}(r) = \frac{n_{ij}(r)}{4\pi r^2 \, \mathrm{d}r \rho_j}. \tag{5}$$

$n_{ij}(r)$ are the number of particles of type j between distances r and $r + \mathrm{d}r$ from a particle of type i, and $\rho_j = c_j \rho_0$. It is common to use either of two additional correlation functions as alternative representations to $G(r)$: the differential correlation function, $D(r)$, and the total correlation function, $T(r)$, defined as:

$$D(r) = 4\pi r \rho_0 G(r) \tag{6}$$

$$T(r) = 4\pi r \rho_0 \left[G(r) + \left(\sum_{i=1}^{n} c_i \overline{b}_i \right)^2 \right]. \tag{7}$$

These equations can be adapted for x-ray diffraction, as discussed, for example, by Keen [11].

2.2. General RMC method

The RMC method uses the Metropolis Monte Carlo algorithm to produce atomic configurations that are consistent with experimental data. Atoms in the configuration are selected at random and then moved by a random amount. Instead of changing the potential energy of the configuration the fit to the experimental data is used to determine if each move is accepted or rejected. In the traditional RMC approach, either or both of $F(Q)$ or $G(r)$ are compared with experimental data during the minimization process.

The calculated form of $F(Q)$ is obtained by Fourier transformation of $G(r)$ calculated from the RMC configuration, and hence the range is limited by the size of the RMC configuration. The consequence of this limited r range is that the Bragg peaks in the calculated $F(Q)$ will be broadened. Hence, this calculated $F(Q)$ function cannot be compared with the experimental data until the data have been degraded by convolution with a box function defined by the dimensions of the configuration:

$$F_{\text{box}}(Q) = \frac{1}{\pi} \int_{-\infty}^{\infty} F_{\text{expt}}(Q') \frac{\sin L(Q - Q')/2}{Q - Q'} \mathrm{d}Q' \tag{8}$$

where L is the smallest dimension of the RMC configuration and defines the upper limit of the calculated $G(r)$. Hence, in the RMC simulation, it is the broadened experimental $F_{\text{box}}(Q)$ that is compared with the calculated transform of $G(r)$.

The comparison between the calculated functions and experimental data is formalized by defining an agreement function:

$$\chi^2_{\mathrm{RMC}} = \sum_j \chi^2_j \tag{9}$$

where χ^2_j is the agreement factor for data type j. So for the total scattering data we have the following two agreement factors:

$$\chi^2_{F(Q)} = \sum_j \left[F_{\mathrm{calc}}(Q_j) - F_{\mathrm{box}}(Q_j)\right]^2 / \sigma_{F(Q)^2}(Q_j) \tag{10}$$

$$\chi^2_{G(r)} = \sum_j \left[G_{\mathrm{calc}}(r_j) - G_{\mathrm{expt}}(r_j)\right]^2 / \sigma_{G(r)^2}(r_j) \tag{11}$$

where in principle the σ parameters represent standard errors on individual data values.

The RMC method can also incorporate restraints, in which any calculated quantity f^{calc} can be compared with a required value f^{req}. Common examples of such values are bond lengths and bond angles [12, 13], where the former may be required to equal the midpoint of the corresponding peak in $G(r)$ and the latter may equal an ideal angle for a particular type of polyhedra.

Such restraints have been applied to simulations of silica phases, where the values of the Si–O bond lengths are restrained to be kept close to the mean value given by $G(r)$, and the values of the O–Si–O bond angles are restrained to be kept close to the ideal tetrahedral angle [12]. The restraints are used to define a third agreement function:

$$\chi^2_f = \sum_k w_k \left[f^{\mathrm{calc}}_k - f^{\mathrm{req}}_k\right]^2 \tag{12}$$

where w_k is a weighting factor and its value could reflect a desired spread of values of f about the required value, or gives a relative weighting to this restraint with respect to other contributions to χ^2_{RMC}.

Since the RMC method is a stochastic approach it produces configurations with the maximum entropy and thus the maximum disorder allowable within the constraints of the data. In the early stages of minimization from an ordered crystalline starting configuration the method will mainly disorder the atoms; at this point some 'damage' may be introduced into the structure. This 'damage'—such as broken bonds, distorted polyhedra or displaced cations—will mostly be 'healed' later on in the minimization as equilibrium is approached. However, since the weighting of any individual atom is quite low, some damage can remain and may also lead to extended regions of offset atoms. To try to minimize these effects it is often useful to use restraints and constraints to guide the early stages of minimization to produce more physically acceptable configurations.

3. Previous approaches to RMC modelling of polycrystalline materials

The problem of the degradation of the information contained within the Bragg peaks of polycrystalline materials as encapsulated in equation (8) has been tackled using two approaches. The first, due to Mellergård and McGreevy [5] avoids the handling of $G(r)$ completely. Instead, the three-dimensional function $S(\mathbf{Q})$ is calculated from the three-dimensional model:

$$S(\mathbf{Q}) = \left|\sum_j \overline{b}_j \exp\left(\mathrm{i}\mathbf{Q}\cdot\mathbf{r}_j\right)\right|^2 \tag{13}$$

where $\overline{b}_j$ is the coherent scattering length of the jth atom. The values of $\mathbf{Q}$ that can be used are defined by the dimensions of the model. The complete set of values of $S(\mathbf{Q})$ are collapsed onto the one-dimensional projection for a polycrystalline sample and broadened according to the instrumental resolution function to give the calculated $F(Q)$ used in equation (10). The advantage of this approach is that it gives a proper comparison of the Bragg scattering in $F(Q)$. The disadvantage is that the computational demands scale as the cube power of the $Q_{\max}$ value of the data being fitted. Hence, for data with a large maximum Q (such as is obtainable at neutron spallation sources) this approach is not suitable. This method was implemented into the `RMCPOW` program.

An alternative approach has been used [3]. In this approach we extract the intensities of the Bragg peaks from the diffraction data using the Pawley method [14]. We then define a new agreement factor to be incorporated into equation (9):

$$\chi^2_{\text{Bragg}} = \sum_{hkl} \left| |F_{\text{calc}}(hkl)|^2 - s|F_{\text{expt}}(hkl)|^2 \right|^2 / \sigma^2_{hkl} \tag{14}$$

where the structure factor is given in the normal way:

$$F_{\text{expt}}(hkl) = \frac{1}{N} \sum_j \overline{b}_j \exp(\mathrm{i}\mathbf{Q}_{hkl} \cdot \mathbf{r}_j) \tag{15}$$

and $\mathbf{Q}_{hkl}$ is the scattering vector of the hkl Bragg reflection. The parameter s in equation (14) is a scale factor, which is treated as an adjustable parameter in the RMC method (as described in more detail by Tucker *et al* [3]). This approach has been implemented in the program `RMCBragg`, which is based on the original `RMCA` program of McGreevy and Pusztai [1].

The advantages of this approach are that there are no significant computational overheads and that it allows us to take full account of the form of $G(r)$ in the RMC simulation. The main disadvantage is that the overlapping of Bragg peaks in the diffraction pattern means that we cannot make maximum use of the Bragg diffraction information.

4. RMCProfile: a profile refinement approach to the RMC analysis for polycrystalline materials

The disadvantages of the previous approaches have now been overcome by developing a new implementation of the RMC method that incorporates a profile fitting of the Bragg diffraction pattern. In time-of-flight instruments, it is common to reduce the diffraction data to a corrected function of flight time $I_{\text{expt}}(t)$, where t is the neutron flight time. We define a corresponding χ^2 contribution to equation (9):

$$\chi^2_{\text{profile}} = \sum_j \left[I_{\text{calc}}(t_j) - s' I_{\text{expt}}(t_j) \right]^2 / \sigma_{I(i)^2}(t_j) \tag{16}$$

where

$$I_{\text{calc}}(t_j) = \sum_{hkl} L_{hkl} |F(hkl)|^2 R_{hkl}(t_j - t_{hkl}) + B(t_j). \tag{17}$$

L_{hkl} is the Lorentz factor of the hkl reflection, $R_{hkl}(t_j - t_{hkl})$ is the peak shape of the hkl reflection arising from the instrument resolution and $F(hkl)$ is the structure factor of equation (15). s' is a scale factor and $B(t)$ is the background in the diffraction pattern, which arises from the diffuse scattering component of the total scattering. The sum is over all hkl, including symmetry related sets. We also include the hkl values for systematically absent reflections—in so doing we ensure that the RMC simulation is able to reproduce part of the translational symmetry.

The values of s', the coefficients that define $B(t)$, and the coefficients that define $R_{hkl}(t_j - t_{hkl})$ can be obtained by a preliminary analysis of the Bragg diffraction pattern using the Rietveld [7], Pawley [14] or Le Bail [15] methods as incorporated into programs such as GSAS [16]. The same analysis will give the lattice parameters which are needed to construct the initial RMC configuration, and to give the values of the positions of the Bragg peaks, t_{hkl}. The values of s' and $B(t)$ are not adjusted during the RMC refinement process.

The new approach has been incorporated in the program RMCProfile, which is a significant modification of RMCBragg [3]. Additionally, the program has an option to include the resolution function in the calculation of $F(Q)$. This is useful for high-precision studies since without this the fits to $F(Q)$ and the high-r region of $G(r)$ will not be consistent with the fit to the Bragg data (which necessarily include the resolution function). This is because the Bragg peaks are experimentally broadened in $F_{\rm expt}(Q)$ but not in $F_{\rm calc}(Q)$ in equation (10). Also, if $G_{\rm expt}(r)$ is obtained via direct Fourier transformation of $F_{\rm expt}(Q)$, then the instrument resolution will dampen the high-r amplitude and this region of $G_{\rm expt}(r)$ will not agree perfectly with $G_{\rm calc}(r)$ (which is obtained directly from the RMC configuration). This can be overcome by using an inverse method such as MCGRtof [17] to obtain $G_{\rm expt}(r)$ and by convolving $F_{\rm calc}(Q)$ with the instrument resolution in RMCProfile. However, the resolution function correction is computationally costly and it is often preferable to use this facility only in the final stages of an RMCProfile refinement or only for large RMC models (where the box convolution effect is less dominant—see equation (8)).

As with all refinement methods, RMCProfile is only as effective as the quality of the data provided. That said, RMCProfile may provide some physical insight even when applied to data of limited extent, e.g. $F(Q)$ with low $Q_{\rm max}$. However, the best results will always be obtained from RMCProfile refinements of high-quality data sets (e.g. $I(t)$, $F(Q)$ and $G(r)$ refined simultaneously).

5. Additional features of RMCProfile

5.1. Polyhedral restraints

As described earlier it is possible to include additional data-based restraints during an RMC refinement. These are implemented in RMCProfile in the form of polyhedral restraints. At present a number of different polyhedral restraints have been implemented for various combinations of polyhedra and specific molecular configurations. Each restraint is for a specific type of system rather than a generic restraint definable by the user; this has been done for simplicity of coding, the use of existing code and for speed of implementation.

The contribution of these restraints to χ^2 typically has the form given here:

$$\chi^2_{\rm Restraint} = w_{\rm bond} \sum_{\rm bonds} (r_{\rm bond} - R_{\rm bond})^2 + w_{\rm angle} \sum_{\rm angles} (\theta_{\rm poly} - \Theta_{\rm poly})^2 \qquad (18)$$

where $w_{\rm bond}$ and $w_{\rm angle}$ are the weighting of the bond and angle restraints, $R_{\rm bond}$ and $\Theta_{\rm poly}$ are the ideal polyhedral bond distances and angles, respectively, and the summation is over all the bond distances $r_{\rm bond}$ and angles $\theta_{\rm poly}$ in the configurations. It is implicit within this formulation that atoms linked by these restraints cannot move apart without penalty. It is therefore possible to build and maintain a network topology with these restraints, if appropriate.

The weights should be set low enough to ensure that the data and not the restraint determine the final polyhedral shape, otherwise the low-r data in $G(r)$ are effectively ignored. This can be easily checked when fitting the radial distribution function. Figure 1 shows fits to the $T(r)$ function of a system that contains both tetrahedra and octahedra. The fit on the left-hand side

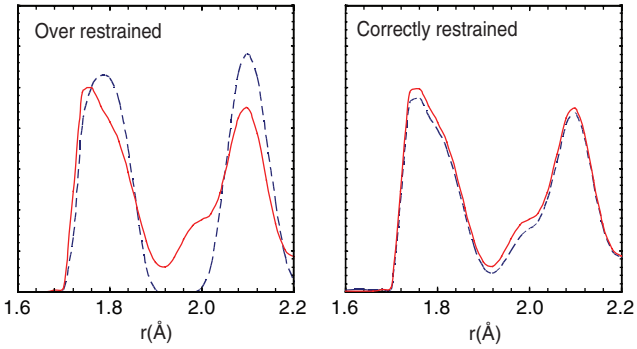

Figure 1. Example of RMCProfile fit (blue dashed line) where the polyhedral restraints has been over-weighted and correctly weighted. The data being fitted (red solid line) is from ZrW_2O_8, the first peak in the distribution describes the distribution of W–O correlations and the second peak the Zr–O correlations.

of the figure was obtained with the restraint weighting set too high and the fit on the right-hand side was obtained after relaxing the weighting sufficiently. With the correct weighting the actual shape of the peaks in the distribution are determined by the data and the restraint simply helps to guide the minimization process.

5.2. Distance window constraint

While the polyhedral restraint is very useful, it is not suitable for all systems, especially when atoms are not in polyhedra or where the aim is to investigate the overall atomic motion in the system such as for phonon calculations (see Goodwin *et al* [18, 19]). For these cases a distance window constraint has been developed, as an extension of the standard closest approach constraint in RMC. This constraint is similar to the 'fixed-neighbour constraints' (FNCs) implemented in `RMC++` [20].

In addition to specifying the closest that two atom types can come together, the user can also specify the furthest that two atom types are allowed to move apart. In this way windows of configuration space are defined within which the atoms are allowed to move. When `RMCProfile` is first run a neighbour list of all the atoms that are within the defined distance windows is generated and this is retained throughout the refinement unless deleted. Hence, the sizes of the windows can subsequently be expanded or reduced but the atoms being constrained by them remain the same.

5.3. Magnetic $S(Q)$ and Bragg profile

The `RMCProfile` program is able to refine magnetic structures, whereby each atomistic configuration is paired with a supercell spin configuration. The positions of the magnetic moments in the spin configuration are determined by the corresponding positions in the atomistic configuration. Each RMC move then involves either a change in atomic position or magnetic moment orientation. The relative frequency ρ_{spin} of each choice is left as a user-definable parameter. It is often useful to employ the special values $\rho_{\text{spin}} = 0, 1$ during the early stages of structure refinement to enable the nuclear and magnetic structures to refine independently. At later stages, an intermediate value (usually $\rho_{\text{spin}} \simeq 0.2$) is used; this value can be refined automatically 'on the fly' via an inbuilt feedback mechanism. Naturally, displacement moves of non-magnetic species do not affect the magnetic scattering

functions, nor do spin displacement moves of magnetic species affect the nuclear scattering functions. Consequently the only significant additional computational cost is the translations of magnetic atoms, whereupon changes in both nuclear and magnetic scattering functions must be calculated.

Spin orientation changes are implemented within `RMCProfile` as follows. The orientation of each spin j is treated as a normalized spin vector $\boldsymbol{\sigma}_j$. A random spin move vector $\mathbf{m}$, whose magnitude $m_{\max}$ determines the maximum change in spin orientation and is determined by the user, is added to $\boldsymbol{\sigma}_j$ and the resultant vector renormalized to give the new spin orientation $\boldsymbol{\sigma}'_j$. The probability distribution associated with this algorithm has its maximum at a move size of $m_{\max}$, and so it is usually appropriate to limit the size of this parameter to a relatively modest value (about 0.1).

In order to calculate the contribution of the magnetic scattering $S_{\mathrm{mag}}(Q)$ to the scattering factor, it is necessary to consider not only the relative positions of each pair of magnetic species, but also the relative orientations of their spins. Such a formalism was given originally by Blech and Averbach [21], and was subsequently developed by Keen and McGreevy [22]. It involves two distinct correlation functions $\langle \boldsymbol{\mu}_x \cdot \boldsymbol{\mu}_x \rangle_r$ and $\langle \boldsymbol{\mu}_y \cdot \boldsymbol{\mu}_y \rangle_r$, which treat those components of the magnetic moment parallel to (subscript x) and perpendicular to (subscript y) the vector that joins the centres of the atoms separated by a distance r. These are treated separately as they give rise to different effects on the scattering function, and are calculated explicitly using the relationship

$$\langle \boldsymbol{\mu} \cdot \boldsymbol{\mu} \rangle_r = \frac{n_{\boldsymbol{\mu}}(r)}{4\pi r^2 \mathrm{d}r \rho c_{\mathrm{M}}}. \tag{19}$$

Here $n_{\boldsymbol{\mu}}(r)$ is the sum of $\boldsymbol{\mu}(\mathbf{0}) \cdot \boldsymbol{\mu}(\mathbf{r})$ for those magnetic atoms whose distance from a central magnetic atom is between r and $r + \mathrm{d}r$, averaged over all magnetic atoms as centres, c_{M} is the concentration of the relevant magnetic species and ρ is the number density of magnetic atoms. The notation of Blech and Averbach uses the two correlation functions:

$$A(r) = \langle \boldsymbol{\mu}_y \cdot \boldsymbol{\mu}_y \rangle_r \tag{20}$$

$$B(r) = [2\langle \boldsymbol{\mu}_x \cdot \boldsymbol{\mu}_x \rangle_r - \langle \boldsymbol{\mu}_y \cdot \boldsymbol{\mu}_y \rangle_r]. \tag{21}$$

These quantities are related to $S_{\mathrm{mag}}(Q)$ by:

$$S_{\mathrm{mag}}(Q) = \frac{2}{3} c_{\mathrm{M}} \left[\frac{e^2 \gamma}{2 m_{\mathrm{e}} c^2} \mu f(Q) \right]^2 + 4\pi \rho c_{\mathrm{M}} \left[\frac{e^2 \gamma}{2 m_{\mathrm{e}} c^2} f(Q) \right]^2 \times \int r^2 \left\{ A(r) \frac{\sin Qr}{Qr} + B(r) \left[\frac{\sin Qr}{(Qr)^3} - \frac{\cos Qr}{(Qr)^2} \right] \right\} \mathrm{d}r, \tag{22}$$

where e, γ, m_{e} and c carry their usual meanings, and μ is the magnetic moment [21, 22]. The first term on the right-hand side of this equation represents the paramagnetic scattering contribution and has no dependency on the orientations of the spins within the sample. The second term is the correlated magnetic scattering contribution. This formalism is readily extended to include contributions from more than one type of magnetic species; one requires a pair of correlation functions $A_{ij}(r)$ and $B_{ij}(r)$ for each pair i, j of magnetic species.

The magnetic contribution to the Bragg intensities is calculated using what is also a standard approach [4]. The key equation is

$$I(\mathbf{Q}) = \frac{1}{N} \left| \sum_j \mathbf{q}_j p_j(Q) \langle \exp(\mathrm{i}\mathbf{Q} \cdot \mathbf{r}_j) \rangle \right|^2, \tag{23}$$

where the magnetic interaction vector $\mathbf{q}_j$ is given by

$$\mathbf{q}_j = \boldsymbol{\sigma}_j - \frac{\mathbf{Q}(\mathbf{Q} \cdot \boldsymbol{\sigma}_j)}{Q^2}. \tag{24}$$

The magnetic scattering amplitudes $p_j(Q)$ are related to the magnetic form factors $f_j(Q)$:

$$p_j(Q) = \frac{e^2\gamma}{2m_e c^2}\mu_j f_j(Q). \tag{25}$$

The Bragg intensities calculated in this way can be converted into a Bragg profile function via equation (17).

5.4. Lattice site disorder

For systems where there is lattice site disorder or vacancies in the structure, moves only involving atom translations may not be sufficient to produce an acceptable atomic configuration of the crystal structure. This is because atoms may not be able to move past neighbouring atoms or indeed will just have to reorder over larger distances than are possible during a realistic minimization run. For these reasons a move which swaps a pair of atoms has been implemented in `RMCProfile`.

The two atom types which may be exchanged are defined by the user together with the ratio of swap moves to translational moves during the RMC minimization. The relative frequency of these moves needs to be tuned to allow enough local relaxation around each atom after a swap move. The exact ratio will depend on the system and the stage of minimization, but typically swapping atoms every fifth move is a good starting value. To ensure this implementation worked correctly various tests were carried out, details of one of these tests is given in the appendix.

5.5. Availability of the RMCProfile code

Further details about the `RMCProfile` method can be found on the RMC website [23] together with the program, documentation, user manual and a set of example files. The website also contains many useful programs for the visualization and analysis of the results from `RMCProfile` refinements.

6. Examples of RMCProfile

While RMCProfile has been under development it has been used to study a number of systems. The requirements of these various systems have driven the developments described in the previous sections. In this section a brief summary of some of these studies is given to illustrate the potential of `RMCProfile` for the analysis of total scattering data.

6.1. The molecular crystal SF_6

`RMCProfile` was first tested on neutron total scattering data obtained from two phases of the molecular crystal SF_6 measured with the GEM diffractometer at ISIS. The disordered phase (96–230 K) has a body-centred cubic structure with one molecule at each lattice point. Below 96 K, the ordered phase has a monoclinic structure with six molecules in the unit cell [24].

RMC refinements of both phases using the program `RMCProfile` were carried out using models of $10 \times 10 \times 10$ unit cells, with lattice parameters obtained from Rietveld refinements using the `GSAS` program. The $\chi^2_{\text{Restraints}}$ functions contained restraints on the S–F bond lengths (values for the required bond lengths being taken from the $D(r)$ functions) and with 90° restraints on the F–S–F bond angles.

The results of this study have been published elsewhere [4]; here only the fits to the data and the resulting configurations are reproduced. Figure 2 shows the $QF(Q)$ and $D(r)$

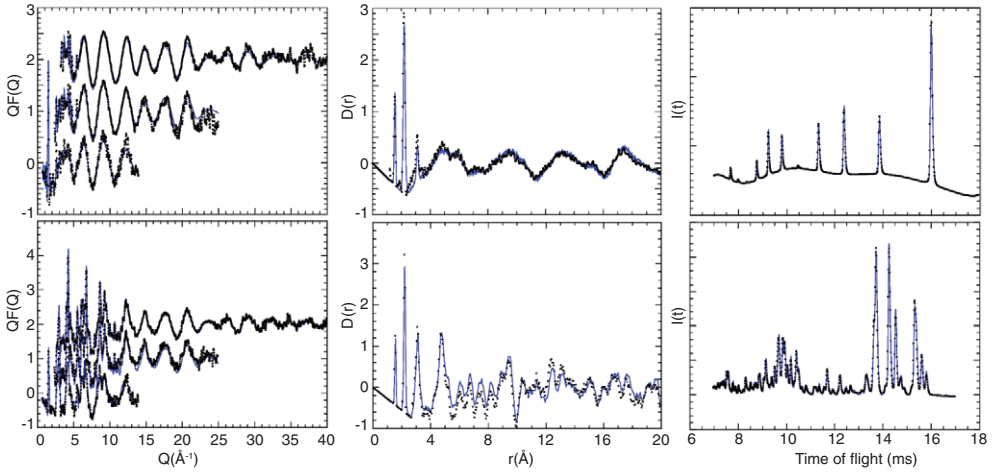

Figure 2. Neutron total scattering structure factor $QF(Q)$ (left), pair correlation functions $D(r)$ (middle) and Bragg profile (right) for the two phases of SF_6 at 190 K (top row) and 50 K (bottom row). The fits obtained using the `RMCProfile` program are shown by the blue solid line. Measurements were obtained using different banks of detectors, and these are shown separately for the $F(Q)$ data.

functions, the diffraction patterns for the two phases of SF_6 and the fits obtained from the RMC refinements. The key point here is that all the data have been fitted simultaneously with the same atomistic model. Slices from the resultant configurations are shown in figure 3.

The slice of the 50 K configuration clearly shows the SF_6 octahedra; their integrity during fitting has been maintained with a polyhedral restraint while their final shape and level of distortion is determined by the fit to the data. It is remarkable that this slice of the configuration shows the correct ordered monoclinic arrangement of the octahedra, especially since RMC is a stochastic method and if it can disorder the octahedra within the constraints of the data it will. The fact that the configuration is highly ordered is entirely due to the data, and particularly due to the inclusion of the Bragg profile in the fitting.

It is perhaps natural to ask if the system is in fact over-constrained with no room for disorder in the models. This may be dispelled by inspection of the configuration slice at 190 K in figure 3. Here the octahedra are still intact but with a high degree of orientational disorder appropriate for the cubic phase of SF_6.

6.2. $SrTiO_3$

Strontium titanate has been the subject of many studies. At room temperature it has a cubic perovskite crystal structure consisting of TiO_6 octahedra linked by their corners, with the strontium cations sitting in the interstices of the TiO_6 network. On cooling below 105 K the structure goes through a displacive phase transition to a tetragonal phase, the result of a $\sim 2^\circ$ octahedral tilt and an accompanying distortion. Pictures of the two average structures are shown in figure 4.

The aim of the `RMCProfile` investigation was to determine if such a small effect could be seen within the configurations, and if so what other information could be gained. The full results of this study were published in the last RMC special edition [25]; here just one of the results is reproduced.

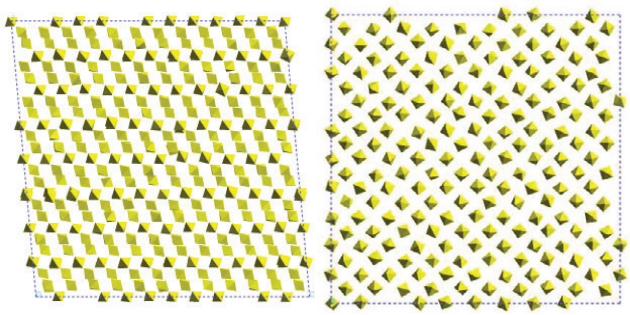

Figure 3. Molecular configurations of the two phases of SF_6 obtained using the RMC program `RMCProfile`. Molecules are shown as octahedra. The configuration on the left is from data for the monoclinic phase at 50 K and the one on the right is from data for the body-centred cubic phase at 190 K.

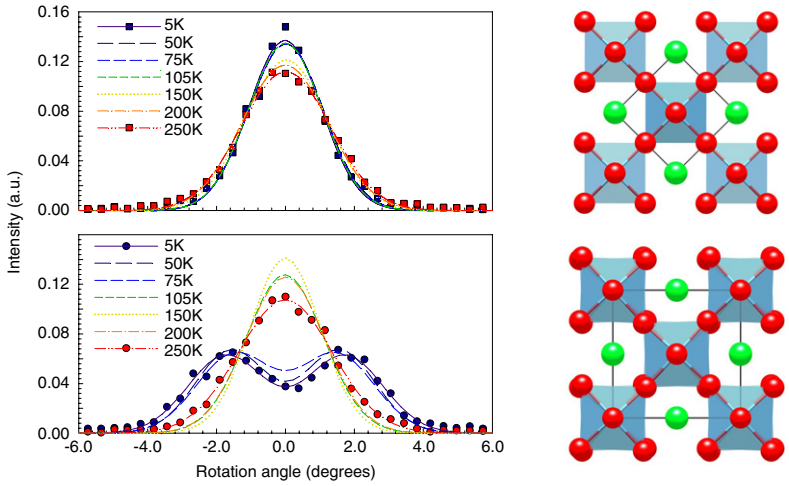

Figure 4. Distribution of TiO_6 rotations as described using geometric analysis. The upper graph shows the x, y rotor distributions, and the lower graph shows the z rotor distributions (figure reproduced from [25]). Crystal structures of the high-temperature (top) and low-temperature (bottom) phases of $SrTiO_3$ are also illustrated, highlighting the TiO_6 octahedra and showing the Sr cations as spheres.

Figure 4 shows the distribution of TiO_6 octahedra in the configurations produced by `RMCProfile` fitting of data from the GEM diffractometer at ISIS collected at various temperatures above and below the phase transition. The distributions were determined using geometric analysis (GA) and by comparing the RMC configuration with an 'ideal' cubic configuration. RMC + GA is a very useful combination and has been used and described by us elsewhere [26]. Here it was used to show the change in, and distribution of, the octahedral tilts in the perovskite structure with temperature. Looking down the x and y directions of the structure there is no tilting of the octahedra, only a distribution due to thermal vibrations centred at 0°. However, looking down the z direction the distribution clearly has maxima at about ±2° below 105 K, and then a single maximum above this temperature as the system has transformed to the cubic structure.

This study showed that RMCProfile could indeed be used to probe very subtle structural changes. The same data were later used to study the phonon modes in the structure; here it turned out that the polyhedral restraints on the octahedra left the Sr atoms to absorb too much of the structural disorder in the early minimization steps. While not a general problem for most studies, when looking for the phonon modes involving the Sr atoms this gave spurious results. It was for this reason we implemented the distance window constraints. When this constraint was used in place of the polyhedral restraint the phonon mode information obtained made much more physical sense. The full details of this study have been published elsewhere [18, 19].

The study of $SrTiO_3$ also encouraged us to study $Ca_xSr_{1-x}TiO_3$. Here there is cation disorder between the strontium and the calcium ions as well as octahedral tilting. We studied three compositions of varying concentration of calcium and strontium. To cope with the large amount of atomic motion required to exchange cation positions we implemented the swap moves algorithm described in section 5.4. This was the first study using RMCProfile to model cation disorder and was a particularly challenging example. This is because the effect of cation ordering on the pair distribution function $D(r)$ is actually quite small due to the overlap of the cation–cation peaks with Ti–Ti and several O–O peaks. Briefly, for the case $x = 0.5$ the RMC predicted a long-range rocksalt-type ordering of the Ca/Sr cations that was confirmed by a subsequent Rietveld refinement. We demonstrated that this is a robust result through running many repeated RMC simulations with quite different initial configurations and different sample sizes. For the cases $x = 0.2$ and $x = 0.8$ long-range order will not be sustained with such large differences in the numbers of Ca and Sr cations, but in the former case the RMC shows significant short-range order and evidence for concentration fluctuations. More details are provided in a separate paper in this special edition [27].

6.3. MnO

The classical antiferromagnet MnO was chosen as an initial case study with which to test the newly implemented magnetic scattering calculations in RMCProfile [28]. This same system had previously been studied using RMCPOW [29], and so serves as an ideal benchmark against which to evaluate the effectiveness of our approach. MnO has been the centre of a large body of systematic magnetic structural investigations that span more than 50 years [30–32]. At room temperature, the material has the rocksalt structure and is paramagnetic. It undergoes a paramagnetic-to-antiferromagnetic transition at a Nèel temperature of $T_N = 118$ K. This magnetic transition is coupled to a structural phase transition, in which the lattice collapses slightly along a single [111] axis to give a low-temperature structure with rhombohedral lattice symmetry. The antiferromagnetic phase is characterized by planes of ferromagnetically aligned Mn spins perpendicular to the unique [111] axis (and hence parallel to the planes themselves), whose alignment direction alternates between successive planes (see inset to figure 5). The magnetic Bragg intensities are sensitive only to the angle between the antiferromagnetic stacking axis and the spin alignment axis, and so the orientation of the spins within the (111) ferromagnetic planes was not known [33].

Total neutron scattering data were collected on a sample of MnO at 10 K using the GEM instrument at ISIS. The data were corrected and normalized following the usual procedures. The RMCProfile code was used to refine atomistic and spin configurations against the experimental $F(Q)$ and Bragg profile functions. The reciprocal space fit obtained is shown in figure 5, where it is compared to that obtained without consideration of the magnetic scattering contribution. A supercell of the known magnetic unit cell, with a volume approximately 1000 times larger than the rocksalt fcc cell of the lattice, was used for the RMC calculations.

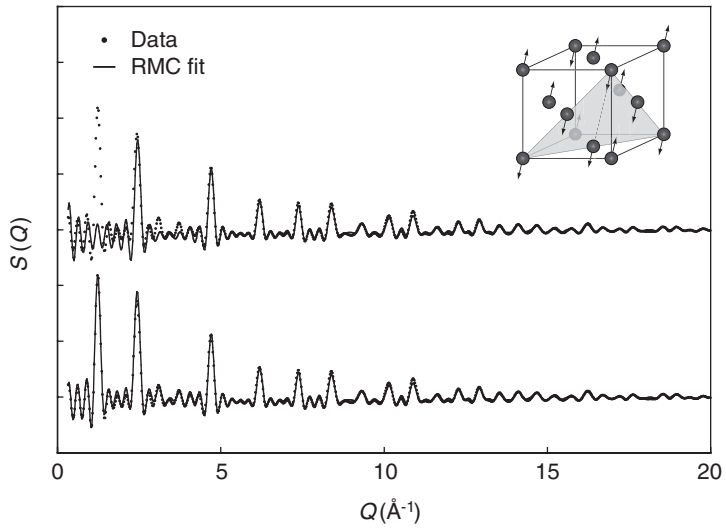

Figure 5. RMC fits to experimental $S(Q)$ data for MnO at 10 K: (top) as calculated from the nuclear RMC configuration alone and (bottom) including the magnetic contribution $S_{\mathrm{mag}}(Q)$ determined from the RMC spin configuration using equation (22). The average magnetic structure of the Mn sublattice is shown in the inset.

The particular choice of cell facilitated the RMC calculations as its axes were orthogonal for arbitrary rhombohedral distortions. Even when started from spin configurations with entirely random spin orientations, the refinement procedure reproducibly yielded equilibrium magnetic structures that showed essentially identical antiferromagnetic alignment patterns that corresponded precisely to the known magnetic structure. In each case the spin directions were aligned perpendicular to the [111] stacking axis, although different runs produced different 'preferred' orientations.

Upon closer analysis, the RMC configurations showed evidence that the rhombohedral lattice symmetry had been broken, albeit only very slightly. It has been known for some time that the magnetic structure of MnO is inconsistent with a rhombohedral lattice, as a spin alignment direction perpendicular to the stacking axis automatically broke the requisite three-fold rotational symmetry. What was observed in the RMC configurations was that the average Mn and O atom positions had systematically shifted from their presumed values in a manner that resembled a frozen-in phonon mode with propagation vector $[\frac{1}{6}\frac{1}{6}\frac{1}{6}]^*$. This distortion gave a monoclinic lattice whose symmetry was commensurate with the associated magnetic structure. Indeed the periodic displacements of the nuclear lattice were observed to be coupled with an out-of-plane spin modulation, which propagated throughout the magnetic lattice with the same periodicity. Moreover, the symmetry lowering seen in this transition potentially allowed some sensitivity in the neutron scattering data to the particular spin alignment direction within the ferromagnetic planes. A very modest but consistent preference was noted for alignment along the $\langle 11\bar{2}\rangle$ directions, which agreed with earlier theoretical predictions.

What emerged from this study was that RMC is potentially a highly valuable tool for investigating the rich and complex information concerning magnetic structure contained within neutron total scattering data. Moreover, the ability to refine magnetic structures using random spin configurations as a starting point avoids the assumption of a particular structural model in the refinement process.

7. Summary

We have reported the development and capabilities of a new RMC method for polycrystalline materials, as incorporated in the new program `RMCProfile`. This new program has been used to successfully model simultaneously the Bragg and diffuse components contained within total scattering data of many interesting crystal systems. This has resulted in models that reproduce both the short-range aspects of the structure together with the long-range crystallographic order. These models have been analysed to gain the maximum amount information from the total scattering measurements. In addition to the examples given in this paper `RMCProfile` has been used to study piezoelectric materials and their thermal development [34]; negative thermal expansion materials and the mechanism of contraction on heating [35, 36]; bond distributions in silica glass [37] and even to extract phonon and spin-wave dispersion curves from powder diffraction data [18, 19, 38]. Clearly the combination of `RMCProfile` and total scattering data is a powerful tool for the study of disordered polycrystalline materials.

Acknowledgments

We are grateful to EPSRC for financial support. We are also grateful to the staff of ISIS for technical support. ALG is grateful to Trinity College, Cambridge for a Research Fellowship.

Appendix

In this appendix we report one test case for the atom swapping algorithm, namely Sr/Ti ordering in the cubic perovskite $SrTiO_3$. In reality the Sr and Ti atoms are perfectly ordered on very different sites, with coordination numbers 12 and 6, respectively. Because we expect no other ordered pattern, and because there is a high contrast between the neutron scattering lengths of the two atomic species (neutron scattering lengths for Sr and Ti are 7.02 and −3.44 fm, respectively) RMC simulations on this example provide a good test of how well the algorithm works.

Experimental data for this test case have been described previously [25]. We took the data for a temperature of 293 K.

To start the tests of the swapping module we used an equilibrated configuration. Figure A.1(a) shows a RMC configuration resulting from a good fit of neutron scattering data of $SrTiO_3$ at 293 K. Ti atoms and Sr atoms are ordered on both long-range and short-range length scales. Ignoring the oxygen atoms, the Ti and Sr atoms are ordered in a CsCl arrangement, each with eight first neighbours of the opposite type and six second neighbours of the same type. The $D(r)$ function and the $n(r)$ values calculated from the configuration are displayed in figure A.1(a).

Our first test was to simply allow the swapping module to rearrange the Sr and Ti atoms at random (unguided by the experimental data, and without atom displacements). The resultant configuration is shown in figure A.1(b). It explicitly shows Ti and Sr atoms exchanged their positions. Figure A.1(b) also shows the significant effects on $D(r)$ and $n(r)$. Note that the first peak in the $D(r)$ function, which corresponds to the ordered Ti–O distance, has swapped from being negative (due to the negative scattering length of Ti) to positive (because Sr has a larger positive scattering length).

Our second test was to see if the swapping procedure will bring the disordered configuration in figure A.1(b) back to the ordered configuration in figure A.1(a). The result of this test is shown in figure A.1(c). The configuration looks very similar to the ordered

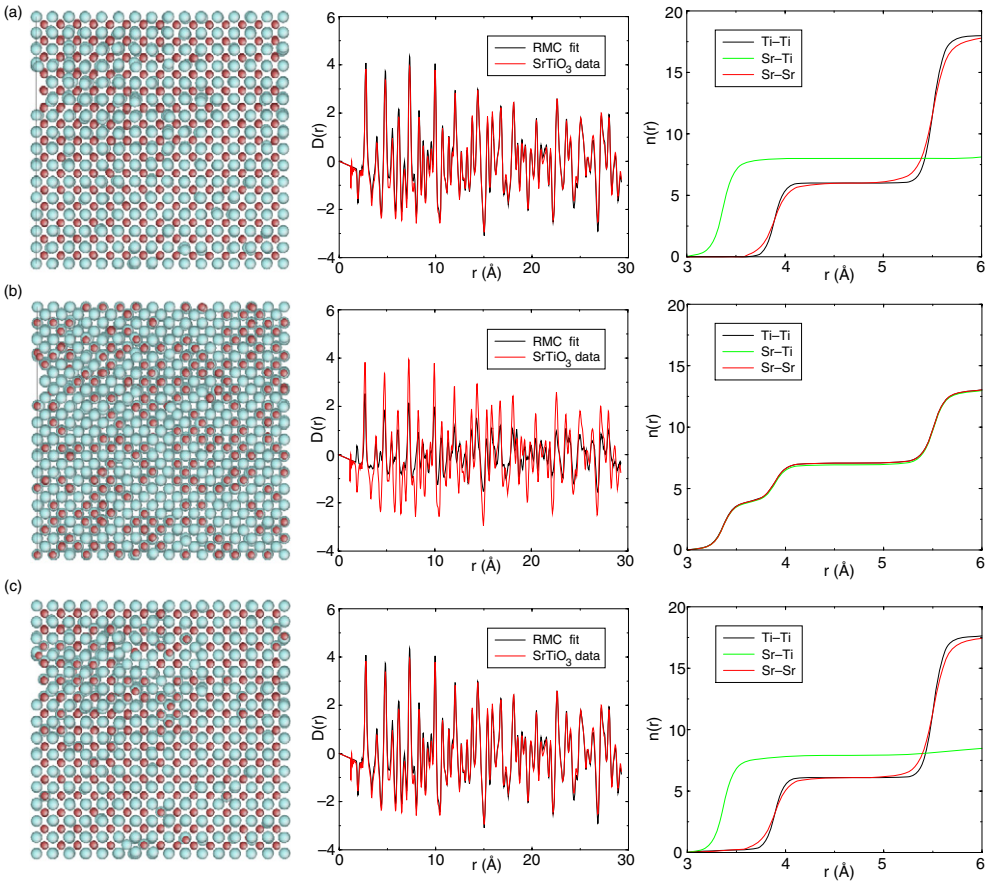

Figure A.1. RMC configurations of $SrTiO_3$ at 293 K (left), with corresponding $D(r)$ (middle) and $n(r)$ (right) functions for models (a) without atom swapping, (b) after the atoms have been allowed to swap at random and (c) after the atoms have been allowed to order following a randomization stage.

structure in figure A.1(a). The $D(r)$ function now fits well (compared with the $D(r)$ functions in figure A.1(a), to which we expect the simulation to converge, and in figure A.1(b), which was the starting point). The $n(r)$ function for the equilibrated configuration shown in figure A.1(b) has returned to being close to that of the initial ordered structure (figure A.1(a)).

References

[1] McGreevy R L and Pusztai L 1988 *Mol. Simul.* **1** 359–67
[2] McGreevy R L 1995 *Nucl. Instrum. Methods* A **354** 1–16
[3] Tucker M G, Dove M T and Keen D A 2001 *J. Appl. Crystallogr.* **34** 630–8
[4] Dove M T, Tucker M G and Keen D A 2002 *Eur. J. Mineral.* **14** 331–48
[5] Mellergård A and McGreevy R L 1999 *Acta Crystallogr.* A **55** 783–9
[6] Keen D A, Tucker M G and Dove M T 2005 *J. Phys.: Condens. Matter* **17** S15–22
[7] Rietveld H 1969 *J. Appl. Crystallogr.* **2** 65–71
[8] Williams W G, Ibberson R M, Day P and Enderby J E 1998 *Physica* B **241–243** 234–6
Day P, Enderby J E, Williams W G, Chapon L C, Hannon A C, Radaelli P G and Soper A K 2004 *Neutron News* **15** 19–23

Hannon A C 2005 *Nucl. Instrum. Methods* A **551** 88–107
[9] Farrow C L, Juhas P, Liu J W, Bryndin D, Bloch J, Proffen T and Billinge S J L 2007 *J. Phys.: Condens. Matter* **19** at press
[10] Egami T and Billinge S J L 2003 *Underneath the Bragg peaks: Structural Analysis of Complex Materials* (Oxford: Pergamon–Elsevier)
[11] Keen D A 2001 *J. Appl. Crystallogr.* **34** 172–7
[12] Keen D A 1997 *Phase Transit.* **61** 109–24
[13] Keen D A 1998 *Local Structure from Diffraction* ed S J L Billinge and M F Thorpe (New York: Plenum) pp 101–19
[14] Pawley G S 1981 *J. Appl. Crystallogr.* **14** 357–61
[15] Le Bail A, Duroy H and Fourquet J L 1988 *Mater. Res. Bull.* **23** 447–52
[16] Larson A C and von Dreele R B 2000 General structure analysis system (GSAS) *Los Alamos Nat. Lab. Rep.* LAUR pp 86–748 unpublished
[17] Tucker M G, Dove M T and Keen D A 2001 *J. Appl. Crystallogr.* **34** 780–2
[18] Goodwin A L, Tucker M G, Dove M T and Keen D A 2004 *Phys. Rev. Lett.* **93** 075502
[19] Goodwin A L, Tucker M G, Cope E R, Dove M T and Keen D A 2005 *Phys. Rev.* B **72** 214304
[20] Evrard G and Pusztai L 2005 *J. Phys.: Condens. Matter* **17** S1–13
[21] Blech I A and Averbach B L 1964 *Physics* **1** 31–44
[22] Keen D A and McGreevy R L 1991 *J. Phys.: Condens. Matter* **3** 7383–94
[23] www.isis.rl.ac.uk/RMC
[24] Dolling G, Powell B M and Sears V F 1979 *Mol. Phys.* **37** 1859–83
[25] Hui Q, Tucker M G, Dove M T, Wells S A and Keen D A 2005 *J. Phys.: Condens. Matter* **17** S111–24
[26] Wells S, Dove M and Tucker M 2004 *J. Appl. Crystallogr.* **37** 536–44
[27] Hui Q, Tucker M G, Dove M T, Redfern S A T and Keen D A 2007 *J. Phys.: Condens. Matter* **19** at press
[28] Goodwin A L, Tucker M G, Dove M T and Keen D A 2006 *Phys. Rev. Lett.* **96** 047209
[29] Mellergård A, McGreevy R L, Wannberg A and Trostell B 1998 *J. Phys.: Condens. Matter* **10** 9401–12
[30] Shull C G and Smart J S 1949 *Phys. Rev.* **76** 1256–7
[31] Roth W L 1958 *Phys. Rev.* **110** 1333–41
[32] Shaked H, Faber J Jr and Hitterman R L 1988 *Phys. Rev.* B **38** 11901–3
[33] Shirane G 1959 *Acta Crystallogr.* **12** 282–5
[34] Haines J, Cambon O, Prudhomme N, Fraysse G, Keen D A, Chapon L C and Tucker M G 2006 *Phys. Rev.* B **73** 014103
[35] Tucker M G, Goodwin A L, Dove M T, Keen D A, Wells S A and Evans J S O 2005 *Phys. Rev. Lett.* **95** 255501
[36] Tucker M G, Keen D A, Evans J S O and Dove M T 2007 *J. Phys.: Condens. Matter* **19** at press
[37] Tucker M G, Dove M T, Keen D A and Trachenko K 2005 *J. Phys.: Condens. Matter* **17** S67–75
[38] Goodwin A L, Dove M T, Tucker M G and Keen D A 2007 *Phys. Rev.* B **75** 075423